NANO LETTERS

pubs.acs.org/NanoLett

Carrier Profiling of Individual Si Nanowires by Scanning Spreading Resistance Microscopy

Xin Ou,[*,†,‡,§] Pratyush Das Kanungo,[*,†] Reinhard Kögler,[‡] Peter Werner,[†] Ulrich Gösele,[†] Wolfgang Skorupa,[‡] and Xi Wang[§]

[†] Max Planck Institute of Microstructure Physics, Weinberg 2, Halle D-06120, Germany, [‡] Institute of Ion Beam Physics and Materials Research, Forschungszentrum Dresden-Rossendorf e.V., P.O. Box 510119, 01314 Dresden, Germany, and [§] Shanghai Institute of Microsystem and Information Technology, Chinese Academy of Sciences, Shanghai 20050, China

ABSTRACT Individual silicon nanowires (NWs) doped either by ion implantation or by in situ dopant incorporation during NW growth were investigated by scanning spreading resistance microscopy (SSRM). The carrier profiles across the axial cross sections of the NWs are derived from the measured spreading resistance values and calibrated by the known carrier concentrations of the connected Si substrate or epi-layer. In the case of the phosphorus ion-implanted and subsequently annealed NWs, the SSRM profiles revealed a radial core—shell distribution of the activated dopants. The carrier concentration close to the surface of a phosphorus-doped NW is found to be by a factor of 6—7 higher than the value in the core and on average only 25% of the implanted phosphorus is electrically active. In contrast, for the in situ boron-doped NW the activation rate of the boron atoms is significantly higher than for phosphorus atoms. Some specific features of SSRM experiments of Si NWs are discussed including the possibility of three-dimensional measurements.

KEYWORDS Nanowire, carrier profile, SSRM, doping, implantation

Because of their unique physical properties, silicon nanowires (NWs) attracted major research interest in the past years.[1,2] One of the most promising applications of Si NWs is their integration in future CMOS circuits to scale down the microelectronics further to nanoelectronics.[3] Two key requirements for applying the NWs in electronic devices and circuits are controlled doping and precise carrier concentration profiling. Controlled doping of NWs has been demonstrated both by in situ doping[4−7] as well as by ion implantation.[8,9] However, in most cases only electrical transport measurements have been used to estimate the active carrier concentrations in the NWs.[4,5,7,9−11] Because of their nanometric size there is a lack of suitable characterization procedures for direct measurement of the active carrier concentration profiles in the NWs. Recently, atom probe tomography[12] was applied to quantify the total concentration distribution of the doping atoms in the NWs. Accumulation of the doping atoms toward the nanowire surface was reported, which shed some light on the dopant incorporation mechanism during in situ doping of vapor—liquid—solid NW growth. However, this method could not quantify the profile of the electrically active dopants in the NWs. Because of its cylindrical geometry and the high surface to volume ratio, the surface of a nanowire plays an important role in determining its electrical properties. One of the most critical surface effects for an unpassivated surface is the segregation of dopant atoms[13] at the Si/SiO_2 interface, which may modify the number of activated dopants in the volume.[13−17] The surface segregation of the active boron dopant in the NWs was reported by Raman scattering[18] and recently by electrical transport measurements in connection with surface etching.[19] Very recently the capabilities of mapping the active dopant concentration in Si NWs were demonstrated by using electron holography.[20] There is clearly an increasing need for direct measurements of the active dopant profile along the cross section of a single NW. In this paper, a direct visualization and quantification of the two-dimensional carrier concentration profiles is demonstrated for doped (both n- and p-type) individual vertical Si NWs of diameter ∼100 nm with scanning spreading resistance microscopy (SSRM).

SSRM[21,22] is based on the contact mode atomic force microscope. A constant force in terms of the deflection voltage is maintained between a conductive tip and the sample, measuring the local spreading resistance in the material in a nanoscale volume. This local spreading resistance is directly proportional to the local resistivity that can be converted to local carrier concentration using the standard carrier concentration versus resistivity curve.[23] The spatial resolution of SSRM mainly depends on the effective contact area between the tip and the sample that is determined by the radius of the tip (several tens of nanometers), the penetration depth into the sample and the nanoroughness of the tip (below 10 nm). Typically, SSRM can achieve a spatial resolution of about 10 nm[21] for a perfectly sharp and fresh tip and has a dynamic range of carrier concentration measured of 10^{15}—10^{20} cm^{-3}.[22]

* To whom correspondence should be addressed. E-mail: (X.O.) X.ou@fzd.de; (P.D.K.) kanungo@mpi-halle.de.

Received for review: 09/29/2009
Published on Web: 12/16/2009

© 2010 American Chemical Society

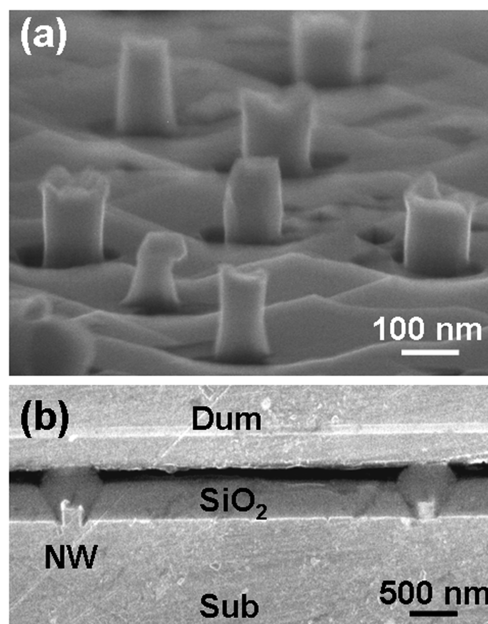

FIGURE 1. (a) SEM image of doped Si NWs with their Au caps removed by wet etching.(b) SEM image of the cross section of a SSRM specimen. The top part denoted as a dummy (Dum) wafer is glued to the sample containing the Si substrate (Sub) and NWs embedded in the SiO_2 matrix.

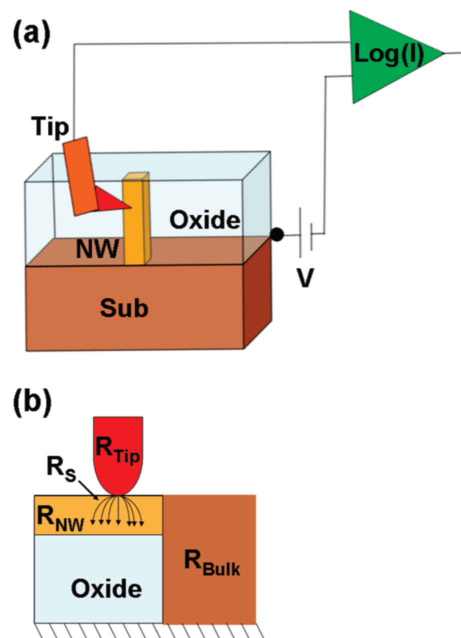

FIGURE 2. (a) Illustration of a SSRM measurement as applied for the investigation of a cross sectional specimen with Si NWs. Log(I) denotes the current amplifier. (b) Different resistors contributing to the electrical circuit.

The NWs of 50 to 250 nm in diameter and 100 to 400 nm in length were grown under ultrahigh vacuum (10^{-10} mbar) in a Riber SiVa45 MBE chamber using Au as the growth-initiator.[24] Doping of the NWs was carried out either by phosphorus ion implantation (for n-type) and subsequent rapid thermal annealing at 1100 °C for 30 s or by boron in situ incorporation during the growth of the NWs at 525 °C (for p-type). The substrate for the n-type NWs was n^+-Si (111) (resistivity ~ 0.001 Ω-cm) and for the p-type NWs p-Si (111) (resistivity ~ 10 Ω-cm). Details of the doping processes including the phosphorus implantation doses and energies are reported elsewhere.[5,9] The expected carrier concentration in the n-type NW was 10^{19} cm^{-3} (see Supporting Information) and in the p-type NW 10^{18} cm^{-3}.[5] Both of the NWs remained fully single-crystalline after doping as confirmed by transmission electron microscopy imaging (see Supporting Information). Figure 1a shows the typical morphology of the vertical Si NWs after removal of the Au droplet (remnants from the Au used for growth initiation) from the top of the NWs by wet etching. Generally, the columnlike NWs stand on an epitaxial layer of thickness of about 300 nm.[24] The grooves observed at the base of the NWs (Figure 1a) are formed due to surface diffusion of Si during the NW growth.[24]

To fabricate the specimen for cross sectional SSRM measurement without removing the NWs from the substrate, a layer of about 400 nm SiO_2 was deposited on the sample by magnetron sputtering to cover the NWs. Subsequently, the specimen was cut and glued by using the same preparation procedures as for the cross sectional transmission electron microscopy except for the Ar ion milling step. The specimen surface was lapped and ground with SiC powder and finally polished with diamond powder. A scanning electron microscopy (SEM) image of an SSRM specimen is shown in Figure 1b.

The scheme of the SSRM measurement is illustrated in Figure 2. An electrical circuit (Figure 2a) consists of the tip, the specimen including the NW embedded in the oxide matrix and the bulk substrate, and of a logarithmic current amplifier to read out the signal. The SSRM measurements were performed using a Veeco multimode atomic force microscope equipped with a conductive diamond coated Si tip. A constant bias voltage of −2.5 V was applied between the tip and the specimen to achieve a reasonable signal-to-noise ratio. The spreading resistance (R_S) comes from a very small volume underneath the tip (Figure 2b), and for an ideal Ohmic contact between a cylindrical tip and a flat sample surface it can be estimated by the formula $R_S = \rho/4a$,[25] where ρ is the resistivity and a is the "electrical radius", that is, the radius of the effective contact area between the tip and the sample. Please note that a can be orders of magnitude smaller than the physical radius of the tip.[26] SSRM is based on the assumption that the spreading resistance R_S is the dominating term in the measured serial resistor R

$$R = R_{Tip} + R_{Bulk} + R_{NW} + R_S \quad (1)$$

where R_{Tip} is the resistance of the probe tip, R_{NW} is the resistance of the Si NW, and R_{Bulk} is the resistance of the

© 2010 American Chemical Society

DOI: 10.1021/nl903228s | Nano Lett. 2010, 10, 171-175

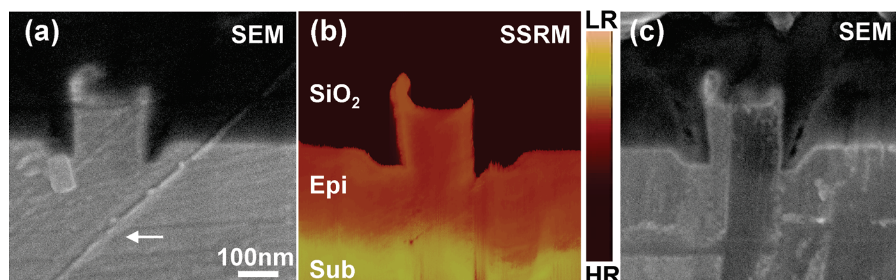

FIGURE 3. (a) SEM image of an individual phosphorus-doped NW before the SSRM measurement. The scratch indicated by an arrow was formed during the sample preparation. (b) Cross sectional SSRM image of the NW shown in (a). Dark and bright colors indicate high (HR) and low (LR) resistance which are scaled on the right side. The NW is connected to the Si substrate (Sub) via a Si epi-layer (Epi). The dark area surrounding the NW is the SiO_2 in which it is embedded. The scanning size is 800 × 800 nm^2. (c) SEM image taken after the SSRM measurement. This NW is the same as the one visible on the left side in Figure 1b.

substrate (including the epi-layer). R_{Bulk} can be neglected due to its very large cross section area as compared to the nanowire. In this case $R_S \gg R_{NW}$ holds $R \approx R_S$ in eq 1, that is, we can attribute the measured resistance entirely to the spreading resistance. The ratio R_{NW}/R_S only depends on the dimensions of the NW (see Supporting Information). It is worth noting that the SSRM images of the Si NW profiles shown in this paper are obtained for the condition of $R_S \gg R_{NW}$ due to the size of the investigated NW cross sections.

Figures 3 presents the SEM images and the corresponding SSRM image of the same phosphorus-doped NW. The consistence of the cross sections of the NW shown by the SEM images before (a) and after (c) the SSRM measurement and of the SSRM image demonstrates the high areal sensitivity of this SSRM measurement. The dark area surrounding the NW indicates the SiO_2 layer with high resistance (HR), and the brighter color shown in the substrate indicates a lower resistance (LR) there due to the high carrier concentration of 7.4×10^{19} cm^{-3} corresponding to its resistivity of 0.001 Ω-cm. The uniform medium dark color shown both in the epi-layer and in the bulk of the NW demonstrated their homogeneous doping to a similar level. This is in agreement with the transport of ions in matter (TRIM) calculations (see Supporting Information). Evidently, there is a brighter colored band at the side wall of the NW shown in Figure 3b. This indicates a lower resistance or higher conductivity there as compared to the bulk of the NW.

Averaged profiles of the spreading resistance (R_S) and carrier concentration in axial (AS) and radial (RS) directions are shown in Figure 4a,b. The R_S data were taken as a 512 × 512 data matrix from a 800 × 800 nm^2 area. R_S was converted to carrier concentration by an appropriate scaling (see Supporting Information) with the known resistivity of the substrate and using the standard carrier concentration vs resistivity curve for silicon.[23] The carrier concentrations along the axial and radial directions to the NW are shown by the right Y axis of Figure 4a,b, respectively. Figure 4a indicates, as expected, that the epi-layer and the bulk of NW are more than 1 order of magnitude less highly doped than the substrate. Figure 4b confirms a higher doping level close to the surface in comparison to the core region of the NW.

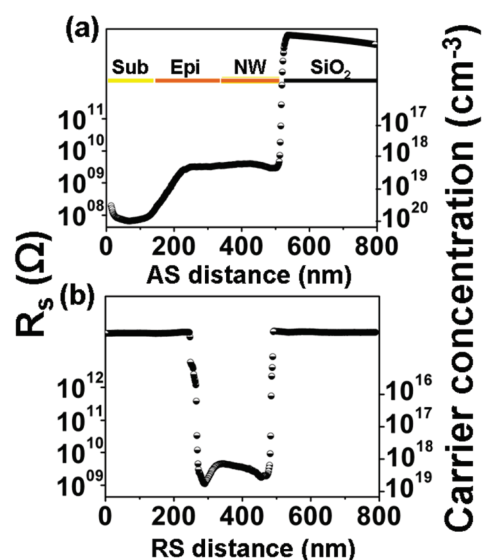

FIGURE 4. R_S profiles extracted from the SSRM image shown in Figure 3b. The profiles in axial direction (AS) and in radial direction (RS) are averaged over the whole Si NW. The carrier concentration (right scale) was converted from R_S values by calibration from the known resistivity (0.001 Ω-cm) of the Si substrate and using the standard carrier concentration vs resistivity curve (ref 23).

The more highly doped region extends from the surface to about 30 nm inside the NW, and the difference between the levels of this shell and the core is about a factor of 6−7. The significant discrepancy between the carrier concentrations of 2.5×10^{18} cm^{-3} average over the whole NW (Figure 4) and the expected average doping level of 10^{19} cm^{-3} is in agreement with recent current−voltage measurements.[9]

The unpassivated outer surface of a NW is normally covered by a thin layer of native SiO_2, and the dopants tend to be segregated at the Si/SiO_2 interface. Phosphorus generally piles up[13,27−31] at the Si/SiO_2 interface. After ion implantation, the redistribution of the phosphorus toward the Si/SiO_2 interface mainly occurs during the rapid thermal annealing and may be enhanced by the implantation damage induced transient enhance diffusion (TED).[28] This redistribution is responsible for the phosphorus loss in the core of the NW. The concentration of the phosphorus atoms in the shell close to the Si/SiO_2 interface can roughly be

© 2010 American Chemical Society

DOI: 10.1021/nl903228s | Nano Lett. 2010, 10, 171-175

estimated to be 1.9×10^{19} cm^{-3} by the assumption that phosphorus in the NW core is fully activated and the phosphorus concentration there is equal to the carrier concentration of 1.4×10^{18} cm^{-3} (Figure 4b). On the basis of this value only about 20% of the phosphorus atoms in the shell close to the surface are electrically active and detected by the SSRM. There is evidently an even stronger dopant deactivation directly at the NW surface. The phosphorus deactivation is due to (i) clustering of segregated dopant in the high concentration region,[31] (ii) dielectric mismatch,[14] and (iii) the surface states existing at the Si/SiO_2 interface of the NW.[11,16] The thickness of the surface region fully depleted by the interface states is calculated according to Seo's model[11] to be 2 nm. However, this thickness cannot be resolved by the present SSRM measurement since the distance between the neighboring data points is 1.6 nm and the spatial resolution is determined to be 4 nm by the measured width of a sharp thermally grown Si/SiO_2 interface.

Another important factor that can influence the dopant profiles in the Si NWs is the existence of the Au remaining from the growth-initiating phase. Au incorporated into the NW may serve as a p-type dopant forming an acceptor state at E_c-0.53 eV in Si and thereby can compensate the n-type carriers induced by phosphorus.[32] Although Au can be found on the surface of the NWs (see the TEM image in Supporting Information), Au incorporated during NW growth is negligible due to the very low Au solubility in Si which is below 10^{15} cm^{-3} at the growth temperature of 525 °C.[33] The Au in-diffusion into the NW during the postimplantation annealing is also limited by the low Au solubility in Si of 2×10^{16} cm^{-3}[33] at that temperature. Such level of Au was detected by Putnam et al.[34] in the volume of the Si NWs grown at 1000 °C by secondary ion mass spectrometry (SIMS). The low concentration restricts the role of Au in carrier compensation in the bulk of the NW by considering the level of the measured carrier concentration. However, the high concentration of the residual Au at the NW surface may contribute the phosphorus deactivation there, for instance, by forming of Au−P complexes.[32]

Figure 5 shows the SSRM image of an in situ boron-doped NW. The respective averaged R_S and carrier concentration profiles (see Supporting Information) in axial and radial directions are given in Figure 6a,b. In this case, the darker substrate implying a higher resistance as compared to the epi-layer and the NW is due to its lower doping level (1.3×10^{15} cm^{-3} corresponding to the resistivity of 10 Ω-cm) as compared to the expected doping level of 10^{18} cm^{-3} in the NW and epi-layer.[5] The dark lines in the epi-layer result from scratches and surface defects induced by mechanical polishing during the specimen preparation. Therefore, there is a strong fluctuation in the carrier concentration of the epi-layer (Figure 6a). It indicates the importance of a highly perfect specimen polishing without mechanical surface defects. In general, the extracted carrier concentrations in the NW (Figure 6) are approaching the expected doping level of 10^{18} cm^{-3}. The carrier profile along the radial direction in Figure 6b is relatively flat as compared to the one shown in Figure 4b indicating that the segregation effect for this investigated boron-doped NW is not as significant as for the phosphorus-doped one. This may result from the 1 order of magnitude lower doping level as compared to the phosphorus-doped NW, from the different doping process, and from the lower segregation coefficient of boron compared to phosphorus.[13] In addition, in contrast to the Figures 3b and 4b, the size of the scanning area in Figure 5 is increased to 2×2 μm^2 and thereby the distance between the data points is increased

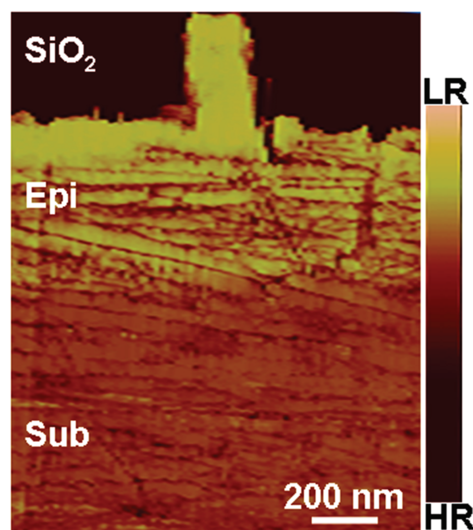

FIGURE 5. Cross sectional SSRM image of an in situ boron-doped NW. Note that the dark lines in the substrate and epi-layer are scratches resulting from the mechanical polishing. The image is taken from a scanning area with a size of 2×2 μm^2.

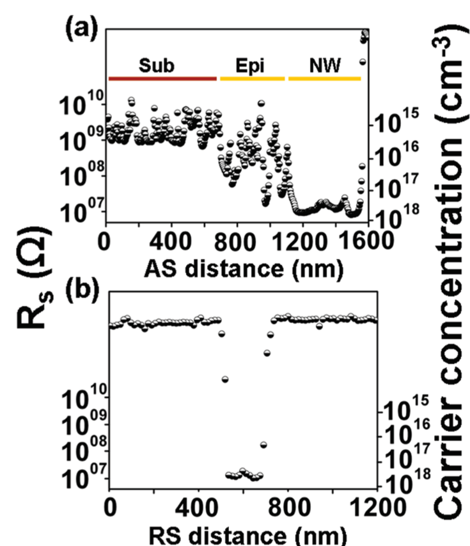

FIGURE 6. R_S profiles extracted from the SSRM image shown in Figure 5. The profiles in axial direction (AS) and in radial direction (RS) are averaged over the whole NW. The carrier concentration (right Y axis) was converted from R_S values by calibration from the known resistivity (0.04 Ω-cm) of the epi-layer and using the standard carrier concentration vs resistivity curve (ref 23).

© 2010 American Chemical Society

DOI: 10.1021/nl903228s | Nano Lett. 2010, 10, 171-175

to 7.8 nm. This reduces the visibility of the effects of dopant segregation and deactivation directly at the NW surface. Nevertheless, the activation rate for boron atoms incorporated in situ during the NW growth is estimated to be 65−70%, which is much higher than for the implanted phosphorus atoms.

Although the investigated NWs here are of larger diameter (∼180 nm) compared to the preferable size for the future logic application. SSRM can be applied for carrier profiling in small diameter NWs (∼10 nm) as well. However, one has to carefully interpret the data as the smaller diameter NWs will have a higher resistance (R_{NW}) that may lead to an overestimation of R_S and affect the accuracy of the extracted carrier concentration from the SSRM measurement. Nevertheless, this effect can be quantitatively considered (see Supporting Information) by a correction approach. It was reported that a spatial resolution as high as 1 nm was achieved in carrier profiling of the ultrashallow junctions by the SSRM characterization in vacuum ambient.[35]

By repeated scanning of the same NW with a controlled force, the tip can abrade some material from the surface of the measured NW cross section. In Figure 3c, the change of the surface after the SSRM investigation is well visible in comparison to the status before (Figure 3a). In this way, the tip gradually moves deeper through the volume of the NW. By measuring the cross sections at different depths of the same NW in succession a three-dimensional (3D) carrier profiling of the NW can potentially be obtained by using an appropriate projection of the two-dimensional profiles along the depth scale. Further investigations regarding 3D SSRM are in progress.

In summary, the electrical properties of cross sections of individual NWs were investigated by SSRM. The carrier profiles of the NWs were determined from the measured spreading resistance with an appropriate calibration by the known resistivity of the underlying Si substrate or the epilayer. Close to the surface region of a phosphorus-doped NW the carrier concentration was found to be higher than in the core. In comparison, the concentration profile of the investigated boron-doped NW shows a higher electrical activation rate of the boron atoms as compared to the phosphorus atoms.

Acknowledgment. The authors gratefully acknowledge Elfi Christalle (FZD) for SEM measurements and Sigred Hopfe (MPI-Halle) for the SSRM specimen preparations.

Supporting Information Available. The analysis of the influence of the nanowire resistance in the spreading resistance measurements, a cross-sectional TEM micrograph of the phosphorus-implanted Si NW with the TRIM simulation, and the calibration technique used to obtain the carrier concentrations from the measured spreading resistance values. This material is available free of charge via the Internet at http://pubs.acs.org.

REFERENCES AND NOTES

(1) Cui, Y.; Zhong, Z.; Wang, D.; Wang, W. U.; Lieber, C. M. *Nano Lett.* **2003**, *3*, 147.
(2) Law, M.; Goldberger, J.; Yang, P. *Annu. Rev. Mater. Res.* **2004**, *34*, 83.
(3) Appenzeler, J.; Knoch, J.; Bjoerk, M. T.; Riel, H.; Schmid, H.; Riess, W. *IEEE Trans. Electron Devices.* **2008**, *55*, 2827.
(4) Cui, Y.; Duan, X.; Hu, J.; Lieber, C. M. *J. Phys. Chem. B* **2000**, *104*, 5213.
(5) Kanungo, P. D.; Zakharov, N.; Bauer, J.; Breitenstein, O.; Werner, P.; Gösele, U. *Appl. Phys. Lett.* **2008**, *92*, 263107.
(6) Wang, Y.; Lew, K. K.; Ho, T. T.; Pan, L.; Novak, S. W.; Dickey, E. C.; Redwing, J. M.; Mayer, T. S. *Nano Lett.* **2005**, *5*, 2139.
(7) Yu, J.-Y.; Chung, S.-W.; Heath, J. R. *J. Phys. Chem. B* **2000**, *104*, 11864.
(8) Hoffmann, S.; Bauer, J.; Ronning, C.; Stelzner, Th.; Michler, J.; Ballif, C.; Sivakov, V.; Christiansen, S. H. *Nano Lett.* **2009**, *9*, 1341.
(9) Kanungo, P. D.; Kögler, R.; Nguyen-Duc, K.; Zakharov, N.; Werner, P.; Gösele, U. *Nanotechnology* **2009**, *20*, 165706.
(10) Ingole, S.; Aella, P.; Manandhar, P.; Chikkannanavar, S. B.; Akhadov, E. A.; Smith, D. J.; Picraux, S. T. *J. Appl. Phys.* **2008**, *103*, 104302.
(11) Seo, K.; Sharma, S.; Yasseri, A. A.; Stewart, D. R.; Kamins, T. I. *Electrochem. Solid-State Lett.* **2006**, *9*, G69.
(12) Perea, D. E.; Hemesath, R. E.; Schwalbach, E. J.; Lensch-Falk, J. L.; Voorhees, P. W.; Lauhon, L. J. *Nat. Nanotechnol.* **2009**, *4*, 315.
(13) Grove, A. S.; Leistiko, O.; Sah, S. H. *J. Appl. Phys.* **1964**, *35*, 2695.
(14) Bjoerk, M. T.; Schmid, H.; Knoch, J.; Riel, S.; Riess, W. *Nat. Nanotechnol.* **2009**, *4*, 103.
(15) Peelaers, H.; Partoens, B.; Peeters, F. M. *Nano Lett.* **2006**, *6*, 2781.
(16) Schmidt, V.; Senz, S.; Gösele, U. *Appl. Phys. A* **2007**, *86*, 187.
(17) Ferna'ndez-Serra, M. V.; Adessi, C.; Blase, X. *Phys. Rev. Lett.* **2006**, *96*, 166805.
(18) Imamura, G.; Kawashima, T.; Fujii, M.; Nishimura, C.; Saitoh, T.; Hayashi, S. *Nano Lett.* **2008**, *8*, 2620.
(19) Xie, P.; Hu, Y. J.; Fang, Y.; Huang, J. J.; Lieber, C. M. *Proc. Nat. Acad. Sci. U.S.A.* **2009**, *106*, 15254.
(20) Den Hertog, M. I.; Schmid, H.; Cooper, D.; Rouviere, J. L.; Björk, T. M.; Riel, H.; Rivallin, P.; Karg, S.; Riess, W. *Nano Lett.* **2009**, *9* (11), 3837.
(21) Wolf, P. D.; Geva, M.; Hantschel, T.; Vandervorst, W.; Bylsma, R. B. *Appl. Phys. Lett.* **1998**, *73*, 2155.
(22) Maknys, K.; Douherets, O.; Anand, S. *Appl. Phys. Lett.* **2003**, *83*, 2184.
(23) Pierret, R. F. *Advanced Semiconductor Fundamentals*, 2nd ed.; Prentice Hall: Upper Saddle River, NJ, 2003; p 191.
(24) Werner, P.; Zakharov, N. D.; Gerth, G.; Schubert, L.; Gösele, U. *Int. J. Mater. Res.* **2006**, *97*, 1008.
(25) Schroder, D. K. *Semiconductor Material and Device Characterization*, 3rd ed.; John Wiley & Sons: New York, 2006.
(26) Eyben, P.; Degryse, D.; Vandervorst, W. In *Characterization and Metrology for ULSI Technology*, Proceedings of the International Conference on Characterization and Metrology for ULSI Technology, Richardson, Texas, March 15–18, 2005; Seiler, D. G., Diebold, A. C., McDonald, R., Ayre, C. R., Khosla, R. P., Zollner, S., Secula, E. M., Eds.; AIP Conference Proceedings; American Institute of Physics: Melville, NY, 2005; Vol. 788, p 264.
(27) Schwarz, S. A.; Barton, R. W.; Ho, C. P.; Helms, C. R. *J. Electrochem. Soc.* **1981**, *128*, 1101.
(28) Gfiffin, P. B.; Crowder, S. W.; Knight, J. M. *Appl. Phys. Lett.* **2003**, *67*, 482.
(29) Duffy, R.; Venezia, V. C.; Loo, J.; Hopstaken, M. J. P.; Verheijen, M. A.; Maas, G. C. J.; Tamminga, Y.; Dao, T.; Demeurisse, C. *Appl. Phys. Lett.* **2005**, *86*, No. 081917.
(30) Chang, R. D.; Tsai, J. R. *J. Appl. Phys.* **2008**, *103*, No. 053517.
(31) Schroer, E.; Uematsu, M. *Jpn. J. Appl. Phys.* **1999**, *38*, 7.
(32) Weman, H.; Henry, A.; Begum, T.; Monemar, B.; Awadelkarim, O. O.; Lindstrom, J. L. *J. Appl. Phys.* **1989**, *65*, 137.
(33) Trumbore, F. A. *Bell Syst. Tech. J.* **1960**, *39*, 205.
(34) Putnam, M. C.; Filler, M. A.; Kayes, B. M.; Kelzenberg, M. D.; Guan, Y.; Lewis, N. S.; Eiler, J. M.; Atwater, H. A. *Nano Lett.* **2008**, *8*, 3109.
(35) Zhang, L.; Tanimoto, H.; Adachi, K.; Nishiyama, A. *IEEE Electron Device Lett.* **2008**, *9*, 799.

© 2010 American Chemical Society

DOI: 10.1021/nl903228s | *Nano Lett.* **2010,** *10,* 171-175